Active Filtering and Regeneration System Dedicated to DC Active Traction Substations

Alexandru Bitoleanu[1], Mihaela Popescu[1]

[1]Faculty of Electrical Engineering, University of Craiova, Romania

Abstract *- This paper is focused on the increasing the energy efficiency of a DC-traction substation by transforming it into an active substation being able to ensure both power quality improvement and braking energy recovery. A system for active filtering and regeneration, named SISFREG, is proposed to be connected between the catenary-line and the primary of the traction transformer, via a dedicated transformer. The main component of SISFREG is a shunt active power filter based on voltage source inverter structure, whose control guarantees the keeping of the prescribed voltage on the DC-side and the proper current at the inverter output by the indirect control of the supply current. The DC voltage controller is tuned in accordance with the Modulus Optimum criterion and the grid current controller is tuned by the Symmetrical Optimum criterion. In order to verify the operation of the system and assess its performance, detailed computer simulation studies were conducted using the Matlab/Simulink package. Based on the conceived Matlab/Simulink model of the whole system, the proper operation is confirmed and the good performance of the system during both traction/filtering and regeneration regimes is shown.*

Keywords – *Active filtering; Recovery breaking energy; Active substation; Voltage inverter; Optimal controllers tuning.*

1. INTRODUCTION

In the DC traction systems, the traction substations are fed by the medium voltage three-phase network and usually contain a specific traction transformer and an uncontrolled rectifier. In order to reduce the harmonic distortion of the supply current, a structure of twelve-pulse rectifier is often adopted, consisting of two diode bridges connected in series or in parallel and supplied from two secondary windings of the transformer, one in star connection and the other in delta connection [7], [61]. The common rated DC voltages provided by the rectifier are: 750 V (most trams and metro rail including one in Bucharest); 1500 V (regional express trains and Intercity) and 3 kV (e.g. Slovenian Railways, trains in South Africa) [7], [27], [32], [50], [61].

The traction substations provide the current only in one direction and they have not the capacity to absorb the energy generated during the braking phases of trains. A reversible station has the capacity to allow the active power flow in the both ways. But, the connection to the same transformer, at the medium voltage side, can affect the capability of achieving the function of harmonics filtering and reactive power compensation. Indeed, it is well known that, based on the operating principle of an active power filter (APF), the DC voltage value must be higher than the AC line voltage magnitude. Moreover, the performance of the system, in terms of supply current distortion during the recovery process, depends on the difference between the two voltages [2], [10], [43], [44].

Although the recovering the braking kinetic energy is an old concern of the specialists, the recent developments in the field of power electronics, creates new solving perspectives. The importance of regeneration is given by the need to increase the efficiency and reduce the energy consumption, but also by the amount of energy which can be regenerated [30], [54].

Usually, a small amount of the recovered kinetic energy is reused in the auxiliary services, whereas the remaining energy is sent back to the electrical network and can be used by an accelerating vehicle in the same line section. If there is no other train nearby, the energy surplus leads to increased network voltage and the braking resistors allow the extra energy dissipation. The methods identified so far for braking energy recovery involve either the use of various mobile/stationary energy storage devices [29] or the direct return to the AC-power utility [7], [27], [32], [30], [45], [46], [54].

Besides the high cost solution of energy storage in mobile or stationary devices such as flywheels, batteries and supercapacitors [18], [29], [58], the alternative approach of using energy recovery converters in order to transfer the recovered energy to the AC power grid provides substantial cost benefits [17], [23], [25], [29], [45], [46], [49], [71], [75]. In the HESOP energy recovery system of Alstom, which is operational on a tram line (750 Volts) in Paris Region since 2011, the reversible converter consists of a

thyristor rectifier bridge associated with an IGBT converter [17]. Another commercial solution is the Sitras Thyristor Controlled Inverter (TCI) provided by Siemens to be connected to the substation at the rectifier transformer through an autotransformer [75].

The specialists are unanimous to conclude that the most advantageous solution is to recover the surplus energy in the traction substations and to compensate the current harmonics and reactive power by materializing de "active station" concept [27], [30], [54], [71].

Compared to the reversible stations, the new system called "active substation" uses the new generation of power devices, with high energetic performances (especially Insulated Gate Bipolar Transistors - IGBT) and it allows not only the energy recovery, but also complementary functions, such as: the grid harmonics compensation by operating like an APF; the active compensation of the reactive power; the dynamic compensation of the voltage variations in the medium voltage line; voltage drop limitation in the supply line [71]. Moreover, the adoption of advanced solutions, such as power active compensators, is a present concern, reflected by several achievements in the power structure and control system [8], [33], [59] , [60].

In the case of the DC metro supply networks, the implementation of "high energy efficiency" can bring more quantitative benefits. In this context, two main directions for improving energy performance were identified [27], [54]:

1. The compensation of the current harmonics and possibly of the reactive power, so that TR operates at unity power factor;
2. Recovering, partially or entirely, the braking kinetic energy as electrical energy.

Though the compensation of the current harmonics and reactive power is an old concern materialized simply by passive filters, nowadays, due to the power electronics development and associated digital processing techniques, the use of active power filters represents a viable and much higher performance alternative [8], [19], [25], [33], [38], [59], [72].

The second direction has implications on increasing the energy efficiency even more significant than the first one and can be concretized through the following ways [29], [58], [68]: using the recovered energy by the auxiliary services of the train; sending it in the catenary line to be used by another train in the same catenary section [63], [66]; storing it by various mobile/stationary devices [18], [20], [23], [31], [33], [60], [71]; sending it in the traction substation (TSS) power grid [73], [74], [76].

In [24], the power integration of large urban railway subsystems is discussed and a DC subsystem for catenaries' interconnection is proposed for the energy transfer. It is worth mentioning that sending the recovered energy in the catenary line to be used by another train in the same catenary's section is successfully implemented through traffic optimization strategies [12], [46], [63], [66].

The technical solution chosen by Ingeteam Traction Company involves including a DC voltage elevation stage consisting of a DC-DC converter between the vehicle DC-line and inverter and solves the problem of system operation as both recovery system and APF by using the existing transformer in the substation [45], [46]. However, from technical and economic point of view, there are at least two critical aspects of this solution at very high power levels (over 1.5 MVA) and high currents (over 2000 A). They are related to the reliability of the DC-DC converter and the cost of the two magnetically coupled coils, which should facilitate the zero current switching.

The objective of the paper is the presentation of a filtering and regeneration system (SISFREG) developed through the project number 42/2014, type Partnerships - PCCA 2013, research program PN-II-PT-PCCA-2013-4, which allows the conversion of the DC traction substations in "active substations".

2. ESTIMATION OF BRAKING ENERGY THAT CAN BE RECOVERED IN THE METRO BUCHAREST

The Bucharest double track subway network is 69.25 kilometers long and has 4 metro lines and 51 stations. The average distance between two stations is 1.5 km. The rated voltage of the catenary is 750 V DC. Each TSS has an apparent power of 2.4 MVA, and includes two rectifier groups (RG), each of them connected to the catenary.

A group consists of a traction transformer – TT (D/d, 20(10) kV/650V, 1.2 MVA) and a three-phase diode bridge rectifier – RT. The maximum DC-line voltage is 950 V DC, during regenerative braking regime.

The subway operation park includes 44 Bombardier trains and 33 trains IVA type (with DC motors).

The main traffic characteristics are: the daily average runtime – 16 hours; the period between two trains (depending on line) – 3-7 minutes at the rush hours (7-9.30 and 16-20) and 8-10 minutes the rest of the day.

The Bombardier train is made up of six cars (four motor cars) and has the following characteristics: empty train weight (M_0) - 173.5 tonnes; seats – 216; standing places - 4 passengers/m^2 – 984; 16 squirrel-cage induction motors of 125 kW each one; the maximum acceleration - 1.1 m/s² (at startup, up to speed v_1=25km/h); the acceleration during the service braking – 1.2 m/s^2; the maximum speed - 100 km/h = 27.8m/s; the maximum run speed - 80km/h=22.22m/s; the residual acceleration when reaching 80 km/h - minimum 0.1 m/s^2; the guaranteed service braking distance for a train with the exceptional load of 8 passengers/m^2, on a dry and horizontal railway, when braking from v_0=80 km/h - max. 224 m.

The usable energy necessary for the movement of the train with equivalent mass M_e in the required

conditions is determined based on the traction characteristics, by numerical integration of the motion equation,

$$M_e \frac{dv}{dt} = F_t - F_r \quad (1)$$

The tractive effort (F_t) corresponds to each operation mode (acceleration – constant speed run – braking), respectively (Fig. 1),

$$F_t = \begin{cases} F_{t\max}; v \in (0, v_1] \\ P_{\max} / v; v \in [v_1, v_N] \\ P_N / v_N; v = v_N \\ -F_{t\max}; \text{for braking} \end{cases} \quad (2)$$

The resistance to motion has three components and the following expression [54]:

$$F_r = A + Bv + Cv^2, \quad (3)$$

where the constants A, B and C result from the above imposed conditions, i.e:

$$\begin{aligned} F_{t\max} &= 1.1P_N / v_1 = Ma_p + A + Bv_1 + Cv_1^2 \\ F_{tm} &= P_N / v_{\max} = A + Bv_{\max} + Cv_{\max}^2 \\ a_{res} &= 1/M\left(1.1P_N / v_N - \left(A + Bv_N + Cv_N^2\right)\right) \geq 0. \end{aligned} \quad (4)$$

The following set of values has been adopted:
A=1467.6; B=455.83; C=75; a_{res}=0.18m/s^2.

In the given conditions, the distance between two stations is covered in 91.6 seconds (Fig. 2 and Fig. 3), and the imposed profiles for acceleration and speed are respected. The necessary tractive effort in order to obtain the imposed deceleration is high and its achievement requires a power whose maximum value exceeds three times the rated power of the motors (Fig. 1).

The braking power keeps two times P_N for about 8 seconds. It is obviously that this force cannot be generated by the traction motors, but by the supplementary braking system of the train.

The energy flow in the system shows that the dynamic processes are predominant and that, in braking

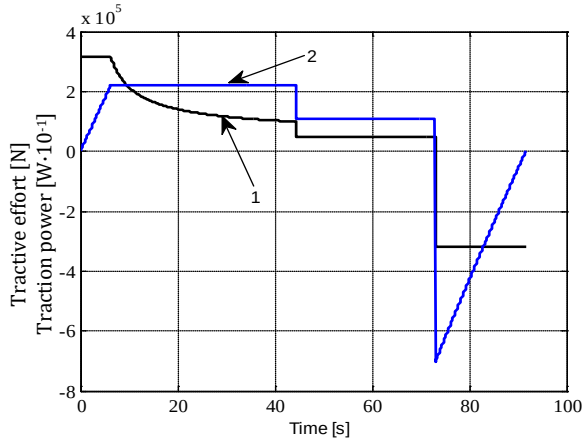

Fig. 1 Tractive effort (1) and its associated power (2) during the train movement between two stations

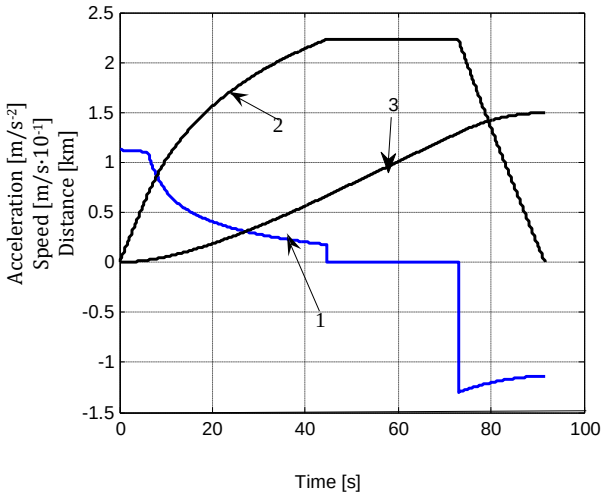

Fig. 2 Acceleration -1, Speed -2 and Distance -3, during the train movement between two stations

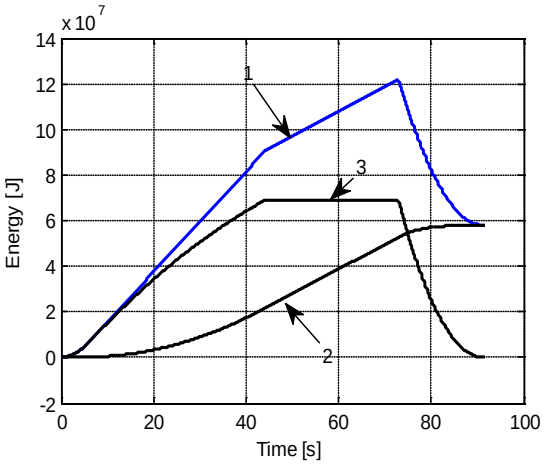

Fig. 3 Energy during the train movement between two stations: 1- associated to the tractive effort; 2- associated to the resistance to movement; 3- kinetic

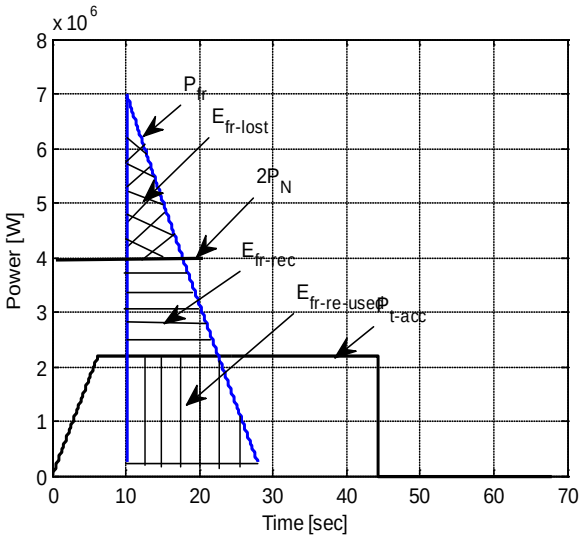

Fig. 4 Braking energy use during the train movement between two stations

mode, the entire accumulated kinetic energy is transferred to the train (Fig. 3).

By overlapping the graphics of the power needed for acceleration and power resulted in the braking process, the quantitative highlight of the possible use of the last one is emphasized (Fig. 4). The analysis is performed by taken into account that the regenerative braking is efficient by the speed of 3 km/h and, during the braking process, it is accepted that the traction motors operate at two times the rated power for about 13 seconds. The following aspects can be emphasized (Fig. 4):

- The energy corresponding to the double hatched area cannot be recovered, because it would overload excessively the traction motors; thus, this energy ($E_{fr\text{-}lost}$) has to be dissipated by other means;
- The vertical hatched energy can be reused by another train that accelerates ($E_{fr\text{-}re\text{-}used}$);
- The horizontal hatched energy can always be sent to the AC power grid;
- If there is no other train accelerating on the same section of the catenary, the energy to be recovered in the AC power grid corresponds to the sum of the two previous areas.

The values of the main quantities are synthetized in Table I and they emphasize the percentage weights for:

- The total energy consumed: 33.86 kWh=100%;
- The total energy from braking: 17.74 kWh=52.45%;
- The lost braking energy: 3.6 kWh=10.63%;
- The maximum energy reused by other vehicle: 8.56 kWh=25.28%;
- The minimum energy that can be recovered by sending it to the power grid: 5.58 kWh=16.48%;
- The maximum energy that can be recovered by sending it to the power grid: 14.14kWh=41.76%.

Considering the average period between two trains of 5 min. at the rush hours (6.5 hours) and of 9 min. for the other hours (9.5 hours), it results that 141 trains are running daily in one station.

A number of 141x51x30=215330 trains corresponds to a total number of the stations of 51 and one month of 30 days. Consequently, considering a recovery efficiency of 90% [13], the energy that can be recovered in the AC power grid, during a month, is minimum 1083.4 MWh and maximum 2745.4 MWh.

The obtained values justify altogether the opportunity of searching specific solutions, such as the active substations. The opportunity is even more evident taking into account that the minimum value corresponds to the perfect timing of the traffic, which is very difficult to accomplish.

Table 1 – Values of the main quantities at the train movement between two stations

Parameter/ Regime	Acceleration	Steady-State (v=constant)	Braking
Time [sec]	44.5	28.5	18.6
Space [m]	657	641	202
Energy for Ft [kWh]	25.3	8.56	-17.74
Energy for Fr [kWh]	-6.06	-8.56	-1.47
Kinetic energy [kWh]	-19.24	0	19.21

3. POSSIBILITIES OF USING THE TRACTION TRANSFORMER IN ACTIVE D.C. TRACTION SUBSTATIONS

The quality of the current injected into the AC-line depends of the difference between the voltage at the DC-side and the magnitude of the line-to-line voltage. The transformer secondary voltage is established provided that the no-load average output voltage of the rectifier (U_{DC0}) ensures the rated catenary's voltage (U_{DCN}) and the voltage drop in the power supply circuit (ΔU), i.e

$$U_{DC0} = U_{DCN} + \Delta U . \quad (5)$$

U_{DC0} depends linearly on the magnitude of the line-to-line RMS voltage in the transformer secondary [17],

$$U_{DC0} = k_R \sqrt{2} U_{st} . \quad (6)$$

Next, we introduced the indicator k_p, as the ratio of U_{DCN} and the magnitude of the line-to-line voltage in the transformer secondary, to characterize the capability of the scheme to allow the regeneration. Thus, as a principle, if k_p is over unity, the scheme is capable of recovery.

If the voltage drop is expressed as a percentage of U_{DCN}, ($\delta U \approx (5 \div 10)\%$), k_p can be expresed as:

$$k_p = U_{DCN} / \left(\sqrt{2} U_{st}\right) = k_R / (1 + \delta U) . \quad (7)$$

k_R is a coefficient depending of the type of rectifier, respectively:

- $k_R = 3/\pi = 0.955$ for the three-phase bridge rectifier and 12-pulse parallel rectifier;
- $k_R = 6/\pi = 1.91$ for the 12-pulse series rectifier.

By particularizing (7) for the three schemes of rectifiers and δU = 0.1, the following results are obtained:

- $k_p = 0.87$ for the three-phase bridge rectifier and 12-pulse parallel rectifier;
- $k_p = 1.74$ for the 12-pulse series rectifier.

It results that only the traction substations with 12-pulse series rectifiers allow the regeneration and compensation by using the traction transformer. In the case of the other two schemes of rectifiers, the regeneration and compensation are possible only by using a dedicated transformer.

Thus, there are two possibilities of connecting the recovery and compensation system to the power supply, i.e.:

- by the existing traction transformer;
- by a dedicated transformer.

4. STRUCTURE OF THE PROPOSED SYSTEM

In setting the structure of the system for regeneration and active filtering, we started from the premise that an IGBT-based APF which is properly

designed and connected is the basic component. Indeed, it has the intrinsic capability to provide an imposed increased value of the DC-bus voltage. On the other hand, ensuring the regeneration function requires the connection to the catenary line by a separating circuit.

Besides APF, the proposed system is composed of (Fig. 5): the separating circuit (SC); the control block (CB); the transducer for the current from DC-line to APF (CT_{CF}); the transducer for the voltage across the compensating capacitor of APF (VT_{CF}). The contactor C_{CF} is used for coupling the DC-line to SISFREG, whereas the contactor C_{AF} allows coupling APF either to the existing traction transformer (TT) or to a recovery transformer (RT).

In the left side, the traction substation is schematized through the traction transformer (TT) coupled to the high voltage supply by the contactor C_{TT} and the uncontrolled rectifier (UR) coupled to the DC-line by the contactor C_{DC}.

For the control of the proposed system, other quantities may be required, such as the voltage and current at the AC side of APF (provided by the transducers VT_{AF}, CT_{AF}) and the voltages and currents at the AC and DC-sides of the traction substation (provided by the transducers VT_A, CT_A, VT_D, CT_D).

The separating circuit must satisfy the following three requirements:

- To achieve an energy buffer between the DC-line and APF, which does not allow the very fast variation of the current;
- To ensure the circulation of the recovery current when requested by the traction motors;
- To ensure the decoupling of APF from the DC-line when there is no recovery current, in order to achieve the function of harmonics filtering and, eventually, the reactive power compensation.

To meet the first requirement, the use of a properly designed inductance, possibly divided into two inductances, for reasons of balancing the circuit, is proposed.

To fulfill the second requirement, the recovery current can be provided naturally by using a diode connected properly.

The capability of the system to operate in filtering and regeneration modes is sustained by the following aspects:

- When the traction motors tend to pass to regenerative braking regime, the rectifier does not allow the existence of a reverse current and, consequently, the DC-line voltage increases;
- The loop of regulation the voltage across the APF's compensation capacitor makes this voltage to be maintained at the prescribed value, with deviations not exceeding 5% [40];
- As long as the DC-line voltage (U_{DC}) is below the compensating capacitor's voltage (U_{DCF}), the separating diode is reverse-biased, the DC-line is practically disconnected from APF and the control block prescribes a compensating current to APF in accordance with the adopted algorithm;
- When U_{DC} exceeds U_{DCF}, the separating diode is forward-biased allowing the existence of the recovering current and the control block prescribes the current to be recovered, which is an active current in phase opposition with the transformer voltage at which APF is connected.

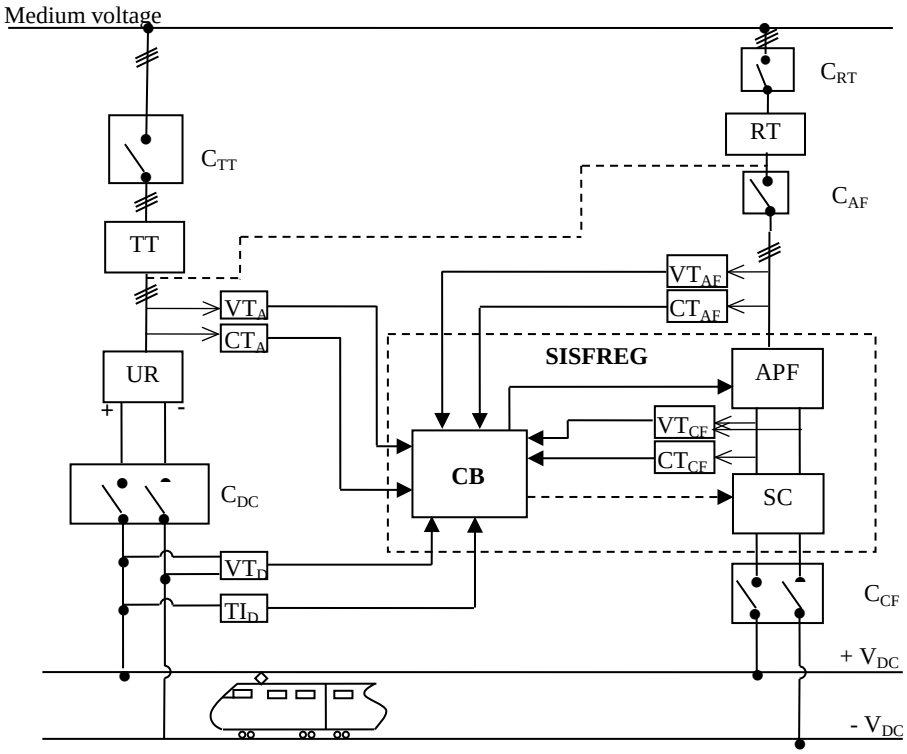

Fig. 5 Block diagram of regeneration and compensation system and its connection

5. DESIGN OF INTERFACE CIRCUITS

5.1. Filter on the AC side

Because the active filter inverter works in switching mode, high order harmonics are added to the compensating current. In order to diminish this effect, the inverter is connected to the AC line through an interface passive filter. It has to accomplish two main criteria:

1. To ensure the current dynamics, by allowing the unaltered passing of the harmonic components which are contained in the reference compensating current;
2. To prevent the spread of the switching frequency harmonics to the power grid.

The structure which leads to high filtering performances is a LCL filter composed of two inductances (L_1, L_2) and one capacitance (C_f). This is more efficient due to the C_f capacitance, being able to satisfy both design criteria. To avoid the oscillations, a damping resistance R_d is added, which is connected, most commonly, in series with the filtering capacitor (Fig. 6). For the design of such a filter, it must be taken into account that the active filtering system can be connected in parallel with the non-linear load, in the point of common coupling (PCC), or through a transformer. The second connection mode is specific to high powers, such as the electric traction substations, when the active filtering system can also perform the function of regeneration the energy recovered in the braking mode to the power grid. Due to the interface filter importance in obtaining high filtering performances, literature often treats the design issue of it, but most often, it is considered the case of voltage inverters that have to provide to the grid a sinusoidal current with the industrial frequency [1], [28], [35], [36], [41], [55], [56], [70].

In our opinion, so far, it was not made a unitary approach based on the damping resistance consideration and on a detailed analysis of each parameter influence.

We consider that, in order to analyze and design an interface filter dedicated to the active filtering systems, the following two aspects must be taken into account: the inverter behaves like a current source, and the interface filter has to be of wideband low-pass type, from the fundamental frequency to the last harmonics intended to be compensated. Consequently, the attention must be focused on the transfer functions related to currents and not on the admittances or impedances [9], [28], [34]-[37], [41], [55], [56], [67].

Moreover, the design criteria have to be directed first on the interface filter performances and then on the energetic criteria (the weight of the interface filter power in the rated power of the filtering system, the voltage drop, etc.) [1], [25], [41].

Equally, it is necessary the detailed analysis of the switching frequency influence relative to the maximum frequency that has to be compensated and to the resonance frequency, because the correlation between them is decisive [37], [67].

Most approaches in the literature, either do not consider the damping resistance [28], [35], [50], [55], [56] or do not highlight the influence of the damping resistance on the losses, although their presence is determined from practical point of view [9], [34], [36], [41].

Not in the least, the LCL filter has some limitations which may lead to finding a design algorithm to achieve the needed compromise in order to obtain good performances. In [27], a critical frequency for the existence of an impedance is identified.

Starting from the equivalent scheme of the filter circuit, at high harmonic frequency, two transfer functions are obtained:

- Output current - input current transfer function,

$$G_1(s)=\frac{I_2(s)}{I_1(s)}=\frac{1+sR_dC_f}{1+sR_dC_f+s^2L_2C_f}; \tag{8}$$

- Filtering capacitor current - input current transfer function,

$$G_2(s)=\frac{I_c(s)}{I_1(s)}=\frac{s^2L_2C_f}{1+sR_dC_f+s^2L_2C_f}. \tag{9}$$

It can see that the transfer functions do not depend on the inductance on the inverter side (L_1) and have the same denominator.

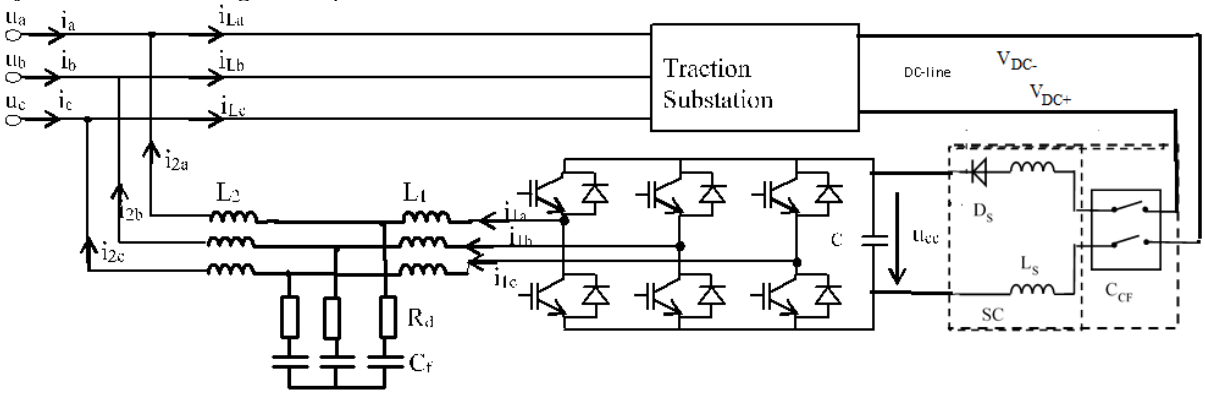

Fig. 6 The shunt active filter structure and the interface filters placement

Depending on the parameters' values, the Bode characteristics of the transfer function G_1 are divided in two categories:

1. The characteristics that have the resonance point located on the left side of the frequency corresponding to the last harmonic to be compensated, respectively $f_{res}<f_N$ (Fig. 7);

2. The characteristics that have the resonance point located between the frequency corresponding to the last harmonic to be compensated and the switching frequency, respectively $f_N<f_{res}<f_{sw}$ (Fig. 8).

It is obviously that the filter performances can not be ideal, but the problem is how its performances can be close to the ideal ones.

From the mathematical point of view, a limitation results from the fact that the transfer function G_1 does not depend independently on the three parameters, but on two combinations of two parameters, respectively $R_d \cdot C_f$ and $L_2 \cdot C_f$. This means that only two equations can be taken into consideration in the filter design and one parameter should be imposed from other reasons.

From practical point of view, for the LCL filter design, the magnitudes corresponding to the two frequencies are imposed (for f_N, $m_N>1$ and for f_{sw}, $m_{sw}<1$) and, eventually, other conditions are added in order to remove the negative effects of the behavior.

After removing the product $R_d \cdot C_f$ between the two conditions, the following expression is obtained:

$$\left(\frac{f_{sw}}{f_N}\right)^2 \frac{1-mp_{sw}}{1-mp_N} = \frac{mp_{sw}(1-\omega_{sw}^2 L_2 C_f)^2 - 1}{mp_N(1-\omega_N^2 L_2 C_f)^2 - 1}. \qquad (10)$$

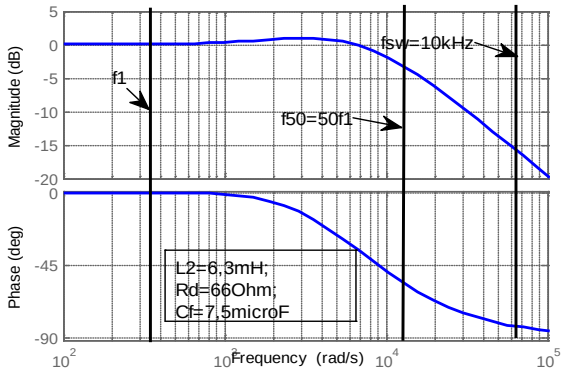

Fig. 7 The frequency characteristics of G_1 in the first case

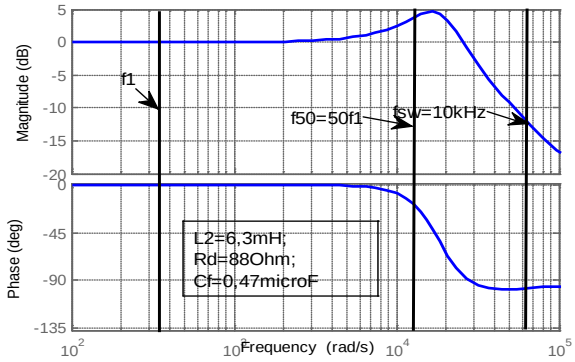

Fig. 8 The frequency characteristics of G_1 in the second case

where mp_N and mp_{sw} are the squares of the magnitudes corresponding to the two frequencies.

The expression (10) shows that the values of mp_N and mp_{sw} are not independent, because the equation has not a positive solution for any combination of the mp_N and mp_{sw} values, when f_N and f_{sw} are imposed. This limitation, maybe the most important, is illustrated in Fig. 9 for f_N=31x50Hz=1550Hz and f_{sw}=10kHz. Moreover, the following aspects are emphasized with reference to Fig. 9:

1. For all values of the magnitudes at frequency f_N, the magnitude at switching frequency decreases as the product $L_2 \cdot C_f$ increases;

2. There is a limit value of $L_2 \cdot C_f$ (about $2x10^{-8}$), for which positive values of the product $R_d \cdot C_f$ exist;

3. The imposed values of m_N and m_{sw} influence each other in a negative way, as for low values of m_N corresponds high values of m_{sw}.

To quantify the extent to which the harmonics to be compensated are influenced by imposing the magnitude response at f_N and f_{sw}, the following magnitude performance indicator penalizing the magnitude of harmonics of low order is proposed:

$$MPI = \sqrt{\sum_{k=1}^{N} \left(|G(j\omega_k)|/k\right)^2 \Big/ \sum_{k=1}^{N} \left(1/k^2\right)}. \qquad (11)$$

Therefore, the more the value of *MPI* is closer to 1, the better filter performance is obtained (Fig. 10).

5.2. Separating Circuit

In order to analyze the system's operation and to conceive the mathematical model of the separating circuit, the equivalent scheme by neglecting the

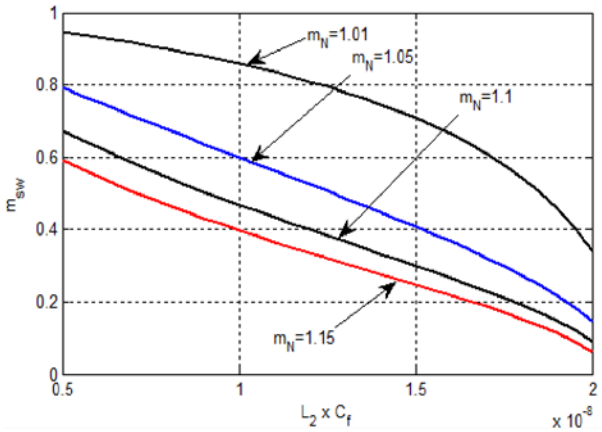

Fig. 9 The magnitude at switching frequency as a function of product $L_2 \cdot C_f$ for four values of the magnitude at f_N .

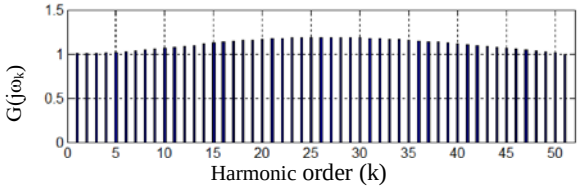

Fig. 10 Magnification of the harmonics up to N=51

resistances of the two inductances and of the traction line-vehicle assembly has been used (Fig. 6).

It must be taken into account that the separating circuit operates only in recovery mode, because in traction mode the diode Ds is reverse-biased by the voltage across the DC-capacitor.

From the point of view of the separating circuit design, the unfavorable situation when switching occurs from the peak value of the line current (I_0) to zero and vice versa is taken into consideration. There will be considered two successive periods corresponding to the switching frequency, i.e. $t \in (0, 2T_s)$. During this time range, the current absorbed by inverter is expressed as:

$$i_i = \begin{cases} 0 & t \in (t_0,\ t_0 + T_s) \\ I_0 & t \in (t_0 + T_s,\ t_0 + 2T_s) \end{cases} \tag{12}$$

Finally, the following expressions are obtained for the current through diode and for the voltage across capacitor:

$$i_d = \begin{cases} \dfrac{E - U_{c0}}{L}\left(t - \dfrac{t^2}{T_s}\right) + I_{d0}; \\ t \in (t_0,\ t_0 + T_s) \\ \dfrac{E - U_{c0}}{L}\left(-t + \dfrac{t^2}{T_s}\right) + I_{d0}; \\ t \in (t_0 + T_s,\ t_0 + 2T_s) \end{cases} \tag{13}$$

$$u_c = \begin{cases} U_{c0} + \dfrac{2(E - U_{c0})}{T_s} t; \\ t \in (t_0,\ t_0 + T_s) \\ 2E - U_{c0} - \dfrac{2(E - U_{c0})}{T_s} t; \\ t \in (t_0 + T_s,\ t_0 + 2T_s) \end{cases} \tag{14}$$

It must be mentioned that the equivalent electromotive force (E) that appears in the above expressions corresponds to the regeneration mode and can be considered as being equal to the rated value of the traction line voltage.

In order to determine the design expressions, the effects of the separating circuit to the DC line-vehicle assembly and to the injected AC-current have been taken into consideration. Consequently, a possible design expression consists of limiting the current ripple in the DC line-vehicle assembly and the ripple of the capacitor voltage (Fig. 11). Their expressions are (per units):

$$\delta I_d = \frac{T_s^2}{4LC_F};\ \delta U_c = \frac{T_s I_0}{2U_{CN} C_F} \tag{15}$$

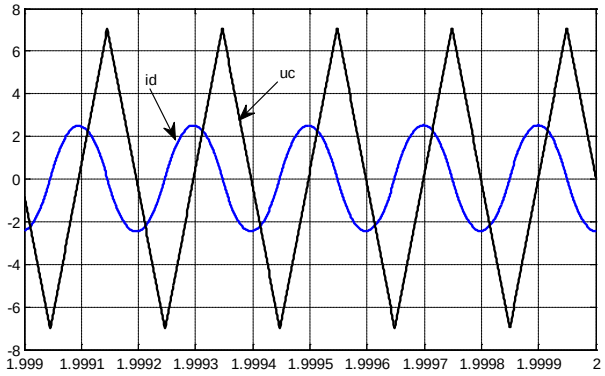

Fig. 11 Waveforms of the DC-line current ripple (p.u.) and voltage across the DC-capacitor ripple (p.u.), in regeneration mode

By imposing the normalized values of the ripples (ε_u, ε_i), the design conditions for each parameter in the DC-link circuit are expressed as follows:

$$C_F \geq \frac{T_s P_{Nrec}}{\eta_r U_{CN}^2 \varepsilon_u};\quad L \geq \frac{\eta_r T_s U_{CN}^2 \varepsilon_u}{4 P_{Nrec} \varepsilon_i}. \tag{16}$$

6. CONTROL OF THE SYSTEM

6.1. Structure of the control system

Usually, the control part of the system contains two closed loops, where the first one is outer and controls the DC voltage and the other is inner and controls the current (Fig. 12). Accurate control of the DC voltage is essential in obtaining good performance of the entire system. Therefore, various solutions have been proposed so far for the control algorithm and for the controller structure [5], [14]-[16], [42], [47], [48], [57], [64]

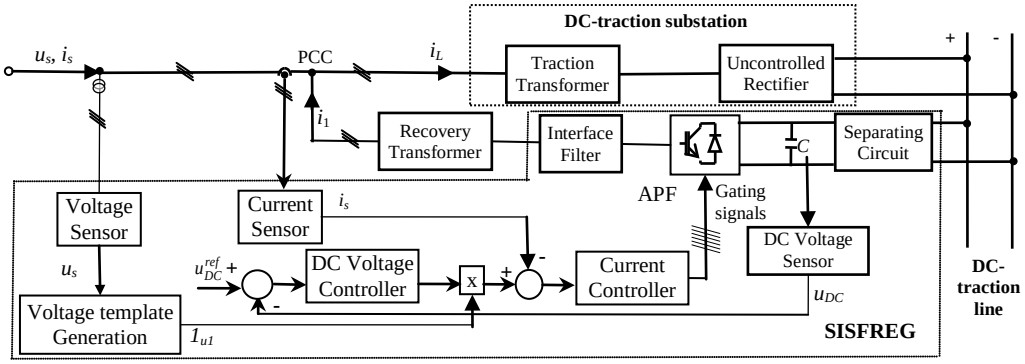

Fig. 12 Single-phase block diagram of the indirect current control-based system

Thus, in [14] and [16], an analysis of different techniques for the control of compensating capacitor voltage is performed. However, there is no argument in favor of a particular method compared with others.

In [43], [48], [57] ,[64] there is a comparative analysis of Fuzzy and PI controller performances. It is concluded that Fuzzy controller leads to better performances. From our point of view, the conclusion is at least questionable, as long as there is no assumption on the correct tuning of the Proportional-Integral (PI) controller.

The sliding mode technique is analyzed in [15] and [47] and the obtained results are similar to the PI controller based results, when the controller is tuned optimally [5].

The hysteresis controllers, which are usually involved in the current control loop, have good dynamic performance, but they do not allow the control of the inverter switching frequency. In order to obtain a constant value of the switching frequency, a lot of improvements were made on the hysteresis controller [3], [6]. For instance, the use of online computation of the variable hysteresis band, Fuzzy techniques [22], [39] or sliding mode [21] are among the proposed solutions.

An interesting PWM method, which includes the sensorless control, is presented in [4].

6.2. Current control methods

Irrespective of the used controller type, the current control involves getting a reference current. Depending on the reference current, two control methods are known: the direct current control (DCC) and the indirect current control (ICC).

In the case of DCC, the reference current is the APF's output current, which, in the filtering/compensation mode, contains the harmonic current to be compensated and, eventually, the fundamental component of the reactive power. Obviously, the comparison is made with respect to the real current at the inverter output.

6.2.1. Indirect current control

ICC involves the grid current control and, therefore, a sinusoidal reference current is compared with the real grid current. It is proved that the active current exchanged by the compensation capacitor with the AC side is directly proportional to the DC-voltage ripple and, consequently, the DC-voltage ripple can be used to estimate the active current [69], [52]. Thus, the reference current can be obtained in two ways. The first one is simpler and consists of multiplying the voltage controller output by three sinusoidal signals of unity magnitude and synchronized with the supply phase voltages. The main advantages of ICC consists of reduced ripple of the controlled current and simplicity of implementation [26]. In addition, when the first way of reference current generation is adopted, it is not necessary to measure the load current. Moreover, the natural transition to the regeneration mode, with notable performances, is allowed [24], [53], [65] , [52].

It must be noted that we substantiated the mathematical support of ICC, for the first time in the literature [13], [52].

Thus, it is proven that the average value of the capacitor current in the period T of the voltage (Fig. 13) has the following expression:

$$I_C = \frac{C \cdot \Delta U_C}{T} \cdot \frac{1-2x}{x(1-x)};\ x = \left(t_M - t_{m0}\right)/T\,. \qquad (17)$$

Expression (17) highlights the following aspects:

- The active current exchanged by the compensation capacitor with the AC power supply is directly proportional to the DC-voltage ripple and, consequently, the DC-voltage ripple can be used to estimate the active current;
- The capacitor absorbs active current (i.e. active power) when $x \in (0, 1/2)$, which corresponds to regime of filtering-compensation;
- The capacitor delivers active power when $x \in (1/2, 1)$, which corresponds to regime of regeneration.

Obviously, the conditions outlined above characterize the two regimes in mathematical terms and they result from physical operation conditions. Thus, the regeneration regime is obtained only if an external source provides active power to the compensation capacitor, as is the case of DC-traction vehicles during the regenerative braking.

On this basis, the structure of the control system was conceived, as shown in Fig. 14.

Based on the prescribed and sensed values of the voltage across the capacitor, the voltage controller of proportional-integral (PI) type gives the magnitude of the reference supply currents. A specific circuit provides three sinusoidal signals (1*ua*, 1*ub*, 1*uc*) of unity magnitude and synchronized with the supply phase voltages, denoting the shapes of the reference currents. The operation of the adopted circuit of phase-locked loop (PLL) is based on the cancellation of an internal fictitious power [62]. It must be stated that the output signals are in phase with the fundamental components of the input voltages, allowing the proper operation even under nonideal voltages.

In the second way, the reference grid current is generated as an active current based on the sensed supply voltage and load current plus an additional component to cover the power losses [53] , [62] , [65], [69], [52].

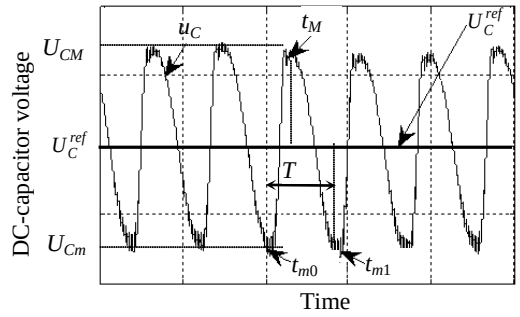

Fig. 13 Typical evolution of voltage across the DC-capacitor and its prescribed value

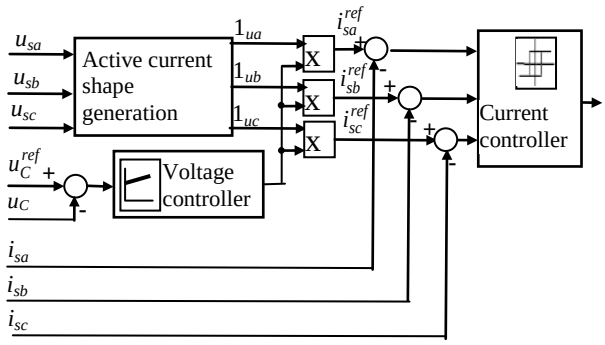

Fig. 14 Block diagram of the indirect current control

Several methods have been used for the generation of the active current, such as p-q theory, synchronous reference frame, FBD theory, Current Physical Components (CPC), and Conservative Power Theory (CPT). The operation under two types of voltage conditions (sinusoidal and distorted) has been taken into consideration. The three compensation goals taken into account were: selective harmonics cancellation; perfect harmonics cancellation; unity power factor. A dedicated Simulink library has been created, in order to be integrated on an experimental platform dSPACE DS1103 [51].

7. OPTIMAL CONTROLLERS DESIGN IN INDIRECT CONTROL

In the adopted cascaded control loops with PI controllers, the DC-capacitor voltage controller output is the reference current magnitude of the grid current controller (Fig. 14) during both filtering and regeneration modes. The difference during operation is given by the output signal sign, which gives the direction of the active power flow, that is: "+" when the vehicle operates in traction mode and SISFREG in filtering mode; "-" when the vehicle operates in braking mode and SISFREG in regeneration mode.

The sinusoidal signals of unity magnitude (1_{uA}, 1_{uB}, 1_{uC}), which are the system's "voltage template", having the same phase as the fundamental voltages, are provided by a specific PLL circuit.

In order to obtain the desired grid current, the IGBTs' gating signals are obtained in two stages. Thus, in the first stage, a current controller processes the input error current and provides a signal containing information about IGBTs' control. Then, this signal is processed and transformed into concrete gate signals for each IGBT through the so-called modulator.

The block diagram of the control system emphasizes the control loops, in which the current loop is inside the voltage loop (Fig. 15). The involved transfer functions are associated to the different parts of the system:

$G_{Fi}(s)$ – the first partial transfer function of the system APF-recovery transformer, from the inverter's control voltage to the AC grid current upstream PCC (it corresponds to the fixed part);

$$G_{Fi}(s)=\frac{I_s(s)}{U_{Ri}(s)}=\frac{U_{DC}K_{TR}}{2R_kU_{r\max}}\frac{1}{(1+T_ks)}=\frac{K_{Ai}}{1+T_ks} \quad (17)$$

$G_{Fu}(s)$ – the second partial transfer function of APF, from the AC grid current upstream PCC to the voltage across the capacitor on the inverter's DC-side;

$$G_{Fu}(s)=\frac{U_{DC}(s)}{I_s(s)}=\frac{\sqrt{3}U_1}{CU_{DC}\cdot s}=\frac{1}{K_{Au}\cdot s} \quad (18)$$

$G_{Ru}(s)$ – the transfer function of the voltage controller;

$$G_{Ru}(s)=K_{Pu}\left(1+\frac{1}{T_{Iu}\cdot s}\right)=\frac{1+\theta_{1u}\cdot s}{\theta_u\cdot s} \quad (19)$$

$G_{Ri}(s)$ - the transfer function of the current controller;

$$G_{Ri}(s)=K_{Pi}\left(1+\frac{1}{T_{Ii}\cdot s}\right)=\frac{1+\theta_{1i}\cdot s}{\theta_i\cdot s} \quad (20)$$

$G_{Ti}(s)$ - the transfer function of the current transducer;

$G_{Tu}(s)$ - the transfer function of the voltage transducer.

$$G_{Ti}(s)=\frac{K_{Ti}}{1+T_{Ti}\cdot s};\ \ G_{Tu}(s)=\frac{K_{Tu}}{1+T_{Tu}\cdot s} \quad (21)$$

The PI current controller is designed using the Modulus criterion which leads to very good

performances for fast systems [40]. The following parameters are obtained:

$$\theta_{1i} = T_k; \quad \theta_i = 2K_{Di}T_{Ti} \tag{22}$$

Since the transfer function of the direct path has a simple pole in origin, the voltage controller was tuned through the Symmetrical Optimum criterion [40]. The following parameters are obtained:

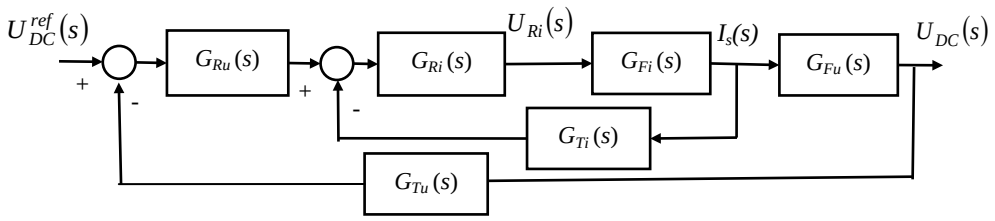

Fig. 15 Block diagram of closed-loop control system based on ICC

$$\theta_u = 32K_{Du}T_{Ti}^2; \quad \theta_{1u} = 8T_{Ti} \tag{23}$$

In the above expressions, K_{Di} and K_{Du} are the amplification factors of current and voltage open loops.

$$K_{Di} = K_{Ai}K_{Ti}; \quad K_{Du} = \frac{K_{Tu}}{K_{Ti}K_{Au}}. \tag{24}$$

8. CONTROL SYSTEM PERFORMANCE

The control system performance was tested in the case of connecting the filtering and regeneration system to a DC-traction substation with 12-pulse parallel rectifier, having the traction transformer in Y/y/d connection and the following rated data: S_N=3.2 MVA; U_{1N}=33kV; U_{2N}=1.2kV [69].

The rated and maximal values of the DC traction line voltage are U_{CN}=1500V and U_{Cmax}=1900V, respectively.

The recovery transformer needed to connect SISFREG in PCC has Y/y connection, S_{Nr}=2.2MVA, U_{1N}=820V, and U_{2N}=33kV. Other quantities involved in the controllers' parameters computation are shown in Table 2. The resulted parameters in the control loops design are: K_{pi}=67.6; T_{Ii}=2.61·10^{-4} s for the current controller; K_{pu}=16.9; T_{iu}=2.93·10^{-4} s for the voltage controller.

The analysis of the control system performance was made by using the conceived Matlab/Simulink model of the whole system, taking into account the real operation conditions (the capacitor charging, the transducers' presence, the sampling period limited to 20 μs, the inverter switching, etc.).

The evolution of the voltage across the compensating capacitor during the charging process, and then the operation in filtering mode, emphasizes the following aspects:

- The charging occurs in three stages (Fig. 16): first the capacitor is charged freely through current limiting resistances (up to 950 V at t = 0.12 s); then, in direct mode, the capacitor voltage reaches the value of 1130 V; in the third stage, the control system starts operating by prescribing a ramp voltage, and the achieved capacitor voltage in quasi-stationary regime is of about 1700 V;
- The charging process in finished in about 0.26s, with an overshoot of about 1.2%; then, the voltage oscillations are lower than 0.5% (Fig. 16).

When changing the operating mode, the voltage loop dynamics is illustrated by the voltage variation over an entire cycle, meaning charging - filtering - regenerating - filtering (Fig. 17). As it can be seen, when passing from the filtering mode to the regeneration mode, the capacitor voltage increases by about 3.5% and

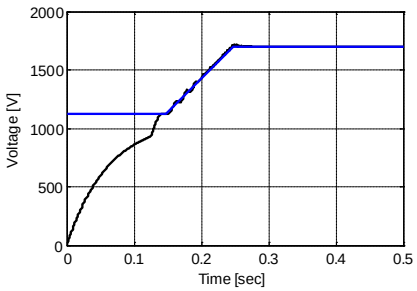

Fig. 16 DC-capacitor voltage during the charging process: prescribed (blue line); real (black line)

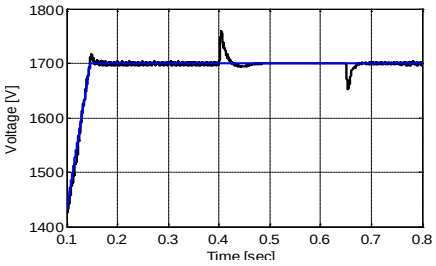

Fig. 17 Voltage across the DC-capacitor during charging-filtering-regeneration-filtering regimes: prescribed (blue line); real (black line)

the steady state regime is reached after an oscillation with very low negative values (about 70 ms).

Returning back to the filtering mode, the voltage across the capacitor decreases by about 2.5% and reaches the steady state regime after about 25 ms.

9. PERFORMANCE OF SISFREG (BUCHAREST METRO CASE STUDY)

The SISFREG's performance was determined using the conceived Simulink model of the whole system, consisting of the SISFREG closed loop system, TSS and vehicle-catenary line assembly.

The model of the vehicle-catenary line assembly, in braking energy recovery mode, includes a braking acceleration control loop having at its input the reference acceleration and the actual acceleration which is proportional to the DC current generated by the vehicle. The output of the acceleration controller means the e.m.f. equivalent to the traction motors in the braking energy recovery mode (modeled as a controlled voltage source). In this way, the reference current is calculated so as to ensure the imposed braking deceleration.

In active filtering mode, the indirect current control technique was adopted [53]. The associated energetic performances (Table 3) and the grid current waveform (Fig. 18) illustrate the correctness of the SISFREG operation. It can be seen that the grid current becomes sinusoidal, having the same phase as the supply voltage.

The resulted current distortion is only 2.22%, which means a filtering efficiency (*FE*) of about 12.

Table 2 – Parameters involved in controllers' design

K_{TR}	R [Ω]	L [H]	U_{Rmax} [V]	C [F]	K_{Tu}	T_{Tu} [s]	K_{Ti}	T_{Ti} [s]	U_{DC} [V]
820/33000	$12.8 \cdot 10^{-3}$	$0.226 \cdot 10^{-3}$	10	$70 \cdot 10^{-3}$	10/2000	$6.18 \cdot 10^{-4}$	10/100	$6.18 \cdot 10^{-4}$	1700

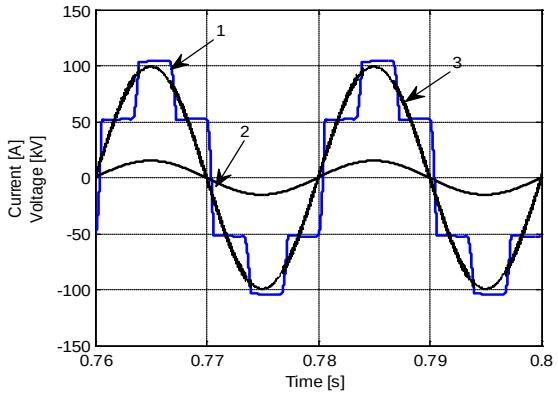

Fig. 18 Load current -1, voltage- 2 and grid current- 3 during acceleration (P=1.1PN) in the presence of APF

Table 3 – Main energetic performances on the grid side during acceleration and operation in filtering mode

P_c [MW]	P_1 [MW]	S_1 [MVA]	*PF*	*Eff*	*THDI* [%]	*FE*
2.2	2.301	2.302	1	0.9636	2.22	12

The active power at the grid side increases slightly, due to the APF's losses and, consequently, the efficiency decreases slightly (0.5%).

When the train operates in braking energy recovery mode, respectively SISFREG operates in regeneration mode, very good performances are obtained too, as it can be seen through the waveforms in Fig. 19 and Fig. 20 and the numerical values in Table 4.

Unity power factor is achieved, the grid current is almost sinusoidal (with a slight distortion of about 1.5%) and has an opposite phase relative to the voltage waveform (Fig. 19), because the power flows from the train to the grid. The efficiency of 92.6% justifies the adopted value in section II to estimate the recovered energy.

The DC voltages waveforms (Fig. 20) illustrate also the transient regime, validating the natural transition from one regime to other one, without exceeding the admissible value of the catenary voltage (950 V).

Table 4 – Main energetic performances on the grid side during the braking regime and SISFREG operation in regeneration mode

P_c [MW]	P_1 [MW]	S_1 [MVA]	*PF*	*Eff*	*THDI* [%]
2.2	2.037	2.037	1	0.926	1.5

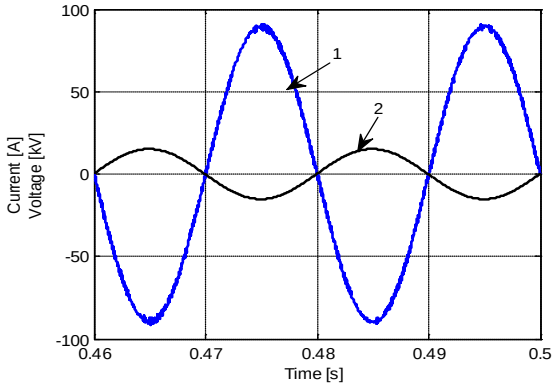

Fig. 19 Current -1 and voltage -2 at the grid side during regeneration

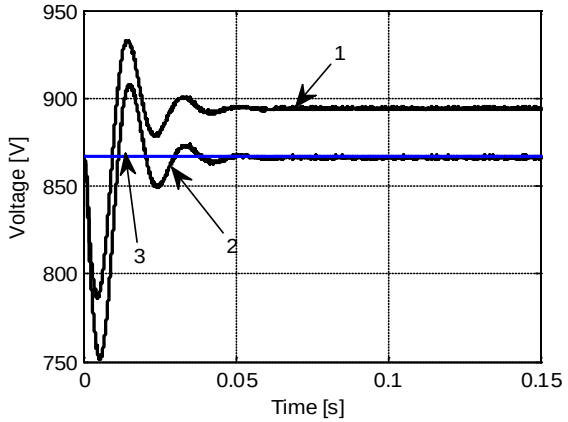

Fig. 20 Catenary voltage -1, compensating capacitor voltage -2 and reference DC-capacitor voltage -3, during regeneration (P=1.1PN)

10. CONCLUSIONS

1. The proposed solution for converting the DC traction substations into active substations involves the use of a power structure consisting of an APF together with a proper separating circuit on the DC-side, called SISFREG. It is shown that the AC-side of SISFREG can be connected directly to the existing traction transformer only when the scheme of traction rectifier is 12-pulse series configuration. In the case of 6-pulse

and 12-pulse parallel schemes, a dedicated power transformer is required to connect SISFREG to the high voltage power supply.

2. Starting from power flow based considerations and practical aspects related to the APF's proper operation, the apparent power of the recovery transformer can be estimated.

3. The regenerated current is practically sinusoidal and in opposite phase with the corresponding supply voltage.

4. The harmonic distortion of the supply current is enclosed in the present standards in both recovery and filtering operation modes.

5. The energetic performances in the recovery mode are notable, the efficiency being over 92%.

6. Good performances are also obtained in the filtering mode, this aspect being proved by the power factor value (about 99.8%, i.e. almost unity power factor) and by the filtering efficiency of about 12.3.

7. It was proved that the proposed system is a viable technical solution for converting DC traction substations in active substations.

8. The analysis performed justifies entirely the need of converting the Bucharest metro TSS into an active TSS. The proposed solution, which also accomplishes the active filtering function, is an option and has to be thorough in terms of the financial aspects.

Actual research is oriented to building an experimental setup and implement the elaborated control algorithms.\

Acknowledgment

This work was performed through the program Partnerships in priority areas — PN II, conducted with the financial support of MEN – UEFISCDI, project no. PN-II-PT-PCCA-2013-4-0564 (42/01.07.2014).

REFERENCES

1. Ahmed K.H., Finney S.J., Williams B.W., "Passive filter design for three-phase inverter interfacing in distributed generation," Electrical Power Quality and Utilisation, vol. XIII, no. 2, 2007.
2. Akagi H., Watanabe H., Aredes M., Instantaneous power theory and applications to power conditioning, Wiley-IEEE Press, 2007.
3. Amer M.R., Mahgoub O. A., Zaid S.A., "New hysteresis control method for three phase shunt active power filter," in Proc. IMECS, vol. II, Hong Kong, March 2011.
4. Angulo M., Ruiz-Caballero D. A., Lago J., Heldwein M. L., Mussa S. A., "Active power filter control strategy with implicit closed-loop current control and resonant controller," IEEE Trans. Ind. Electron., vol. 60, no. 7, pp. 2721-2730, July 2013.
5. Azevedo C.C., Ribeiro R. L. A., Jacobina C. B., Sousa R. M., "DC-link regulator for shunt power active filter using feed-forward control strategy," in Proc. Power Electronics Conference, pp. 877–883, Sept. 2011.
6. Babu G.M., "Simulation study of indirect current control technique for shunt active filter," International Journal of Engineering Research and Applications, vol. 3, no.4, pp.831-851, Jul-Aug 2013.
7. Bae C.H., Han M.S., Kim Y.K., Choi C.Y., "Simulation study of regenerative inverter for DC traction substation," in Proc. ICEMS 2005, vol. 2, Sept. 2005, pp. 1452-1456.
8. Bahrani B, Rufer A., "Optimization-based voltage support in traction networks using active line-side converters," IEEE Trans. on Power Electronics, vol. 28, no. 2, pp. 673 – 685, 2013.
9. Beres R., Wang X., Blaabjerg F., Liserre C.M., "Improved passive-damped LCL filter to enhance stability in grid-connected voltage-source converters," 23rd International Conference on Electricity Distribution Lyon, 15-18 June 2015.
10. Bitoleanu A, Popescu M., Dobriceanu M., Nastasoiu F., "DC-bus voltage optimum control of three-phase shunt active filter system," in Proc. 12th International Conference on Optimization of Electrical and Electronic Equipment, pp. 538 - 543, May 2010.
11. Bitoleanu A., Popescu M., Active Power Filters (in Romanian). Universitaria Craiova, 2010.
12. Bitoleanu A., Popescu M., Dobriceanu M., "Possibilities of using the traction transformer in active DC traction substation," Athens: ATINER'S Conference Paper Series, No: TRA2015-1584, pp. 1-15, Sept. 2015.
13. Bitoleanu A., Popescu M., Suru V., "Optimal Controllers Design in Indirect Current Control System of Active DC-Traction Substation," PEMC 2016, Varna, Bulgaria, in press
14. Blaabjerg F., Teodorescu R., Liserre M., Timbus A., "Overview of control and grid synchronization for distributed power generation systems," IEEE Trans. Ind. Electron., vol. 53, no. 5, pp. 1398-1409, Oct. 2006.
15. Cheng B., Wang P., Zhang Z., "Sliding mode control for a shunt active power filter," in Proc. 3rd International Conference on Measuring Technology and Mechatronics Automation, vol. 3, pp. 282-285, 2011.
16. Choi W.H., Lam C.S. , Wong M.C., Han Y.D., "Analysis of DC-link voltage controls in three-phase four-wire hybrid active power filters," IEEE Trans Power Electron., vol. 28, no. 5, pp. 2180-2191, 2013.
17. Cornic D., "Efficient recovery of braking energy through a reversible dc substation," in Proc. Electrical Systems for Aircraft, Railway and Ship Propulsion (ESARS), pp.1-9, Oct. 2010.
18. Daoud M.I., Abdel-Khalik A.S., Elserougi A., Ahmed S, Massoud A.M., "DC bus control of an advanced flywheel energy storage kinetic traction system for electrified railway industry," in Proc. 39th Annual Conference of the IEEE Industrial Electronics Society, pp. 6596 – 6601, Nov. 2013.
19. Falvo M.C., Sbordone D., Fernández-Cardador A., Cucala A.P., Pecharromán R. R., López-López A.J., "Energy savings in metro-transit systems: A comparison between operational Italian and Spanish lines," in Proc. Institution of Mechanical Engineers, Part F: Journal of Rail and Rapid Transit, vol. 230, no. 2, pp. 345-359, Feb. 2016.
20. Fazel S.S., Firouzian S., Shandiz B.K., "Energy-efficient emplacement of reversible DC traction power substations in urban rail transport through regenerative energy recovery," International journal of railway research, Jan. 2016.
21. Fei J., Li T., Zhang S., "Indirect current control of active power filter using novel sliding mode controller," in Proc COMPEL, pp. 1-6, June 2012.
22. Gadanayak D.A., Panda P. C., "A novel fuzzy variable-band hysteresis current controller for shunt active power filters," ACEEE Int. J. on Control System and Instrumentation, vol. 2, no. 2, pp. 24-28, June 2011.
23. Gelman V., "Energy storage that may be too good to be true: Comparison between wayside storage and reversible thyristor controlled rectifiers for heavy rail," IEEE Vehicular Technology Magazine, vol. 8, no. 4, pp. 70-80, Nov. 2013.
24. Gheorghe L. et al, Hybrid electrical vehicles (Vehicule electrice hibride), Venus, Iaşi, 2006 (in Romanian).
25. Gonzalez-Gil A., Palacin R., Batty P., Powell J.P., "Energy-efficient urban rail systems: strategies for an optimal management of regenerative braking energy," Transport Research Arena, Paris 2014.
26. He L., Xiong J., Ouyang H., Zhang P., Zhang K., "High-performance indirect current control scheme for railway traction four-quadrant converters," IEEE Trans. Ind. Electron., vol. 61, no. 12, , pp. 6645-6654, December 2014.
27. Henning P.H., Fuchs H.D., Roux A.D.L., Mouton H.A.T., "1.5-MW seven-cell series-stacked converter as an active power filter and regeneration converter for a DC traction substation," IEEE Trans. Power Electronics, vol. 23, no. 5, pp. 2230-2236, Sept. 2008.

28. Huang M., Blaabjerg F., Yang Y., Wu W., "Step by step design of a high order power filter for three-phase three-wire grid-connected inverter in renewable energy system," in Proc. 4th IEEE International Symposium on Power Electronics for Distributed Generation Systems, PEDG 2013.
29. Iannuzzi D, Tricoli P., "Speed-based state-of-charge tracking control for metro trains with onboard supercapacitors," IEEE Trans. on Power Electronics, vol. 27, no. 4, pp. 2129–2140, Feb. 2012.
30. Jang S.J., Choi C.Y., Bae C.H., Song S.H., Won C.Y., "Study of regeneration power control inverter for DC traction with active power filter ability", in Proc. 31st Annual Conference of IEEE, IECON 2005.
31. Jung S., Lee H., Kim K., Jung H., Kim H., Jang G., "A study on peak power reduction using regenerative energy in railway systems through DC subsystem interconnection," J. Electr. Eng. Technol ., vol. 8, no. 5, pp. 1070-1077, 2013.
32. Koseki T., "Technical trends of railway traction in the wold," in Proc. International Power Electronics Conference (IPEC), 2010, pp.2836-2831.
33. Lao K.W., Dai N., Liu W.G., Wong M.C., "Hybrid power quality compensator with minimum dc operation voltage design for high-speed traction power systems," IEEE Trans. on Power Electronics, vol. 28 , no. 4, pp. 2024 – 2036, 2013.
34. Li L., Guo Y., Zhang X., "Analysis and application of passive damping LLCL filter in active power filter," in Proc. IEEE CYBER, pp. 751-755, June 2015.
35. Lim S., Choi J., "LCL filter design for grid connected NPC type three-level inverter," International journal of renewable energy research,vol. 5, no.1, 2015.
36. Liu C., Dai K., Duan K., Kang Y., "Application of a C-type filter based LCFL output filter to shunt active power filters," Journal of Power Electronics, vol. 13, no. 6, pp. 1058-1069, Nov. 2013.
37. Liu Q., Peng L., Kang Y., Tang S., Wu D., Qi Y., "A novel design and optimization method of an LCL filter for a shunt active power filter," IEEE Trans. Ind. Electron., vol. 61, no. 8, pp. 4000-4010, Aug. 2014.
38. López-López A.J., Pecharromán R.R., Fernández-Cardador A., Cucala A.P., "Assessment of energy-saving techniques in direct-current-electrified mass transit systems," Transportation Research Part C: Emerging Technologies, vol. 38, pp. 85-100, Jan. 2014.
39. Mahanty R., "Indirect current controlled shunt active power filter for power quality improvement," Electrical Power and Energy Systems, vol. 62 pp. 441-449, 2014.
40. Marin C, Popescu D., Teoria sistemelor și reglare automată, Sitech Craiova 2007.
41. Mejia R. G.E., Munoz N., Cano J.B., "Modeling, analysis and design procedure of LCL filter for grid connected converters," in Proc. IEEE PEPQA, pp. 1-6, 2-4 June 2015.
42. Mekri F., Mazari B, Machmoum M., "Control and optimization of shunt active power filter parameters by fuzzy logic," Canadian Journal of Electrical and Computer Engineering, vol. 31, no. 3, pp.127-134, Summer 2006.
43. Mishra M.K., Karthikeyan K., "An investigation on design and switching dynamics of a voltage source inverter to compensate unbalanced and nonlinear loads," IEEE Trans.Ind. Electronics, vol.56, no. 8, pp. 2802-2810, Aug. 2009.
44. Muszyński M., Mikołajuk K., Toboła A., "Control of dc capacitor voltage in active power filters," Przegląd Elektrotechniczny, vol. 89, no. 4, pp. 245-247, 2013.
45. Ortega J.M., "Ingeber system for kinetic energy recovery & Metro Bilbao experience," Rail Technological Forum for Internationalization, Madrid, June 2011.
46. Ortega J.M.,Ibaiondo H., Romo A., "Kinetic energy recovery on railway systems with feedback to the grid," in Proc. 9th World Congress on Railway Research, May 22–26, 2011.
47. Patjoshi R. K., Mahapatra K. K., "Performance comparison of direct and indirect current control techniques applied to a sliding mode based shunt active power filter," in Proc. IEEE INDICON, 2013.
48. Pavan K.P., Srinivas P. S., Sahu S.K., "Direct & indirect current control of UPQC for enhancing power quality," International Journal of Electrical and Electronics Engineering Research, vol. 5, no. 5, pp. 93-106, Oct. 2015.
49. Pejovic P., Kolar J.W., Nishida Y, "Bidirectional AC-DC converter for regenerative braking," Electronics, vol. 16, iss. 1, pp. 3-8, 2012.
50. Pereira F.H., Pires C. L., Nabeta S. I., "Optimal placement of rectifier substations on DC traction systems," IET Electrical Systems in Transportation, vol. 4, no. 3, pp. 62-69, 2014.
51. Popescu M., Bitoleanu A., "Simulink Library for Reference Current Generation in Active DC Traction Substations," International Journal of Electrical, Computer, Energetic, Electronic and Communication Engineering, vol. 9, no. 8, pp. 578 – 585, 2015
52. Popescu M., Bitoleanu A., Suru V., "Indirect current control in active DC railway traction substations," in Proc. ACEMP-OPTIM-ELECTROMOTION 2015 Joint Conference, Turkey, pp. 192-197, Sept. 2015.
53. Popescu M., Preda A., Suru V., "Synchronous reference frame method applied in the indirect current control for active DC traction substation," in Athens: ATINER'S Conference Paper Series, No: TRA2015-1552, pp. 1-14, June 2015.
54. Randewijk P.J., Enslin J.H.R., "Inverting DC traction substation with active power filtering incorporated," in Proc. Power Electronics Specialists Conference, vol.1, 1995, pp. 360-366.
55. Renzhong X., Lie X., Junjun Z., Jie D., "Design and research on the LCL filter in three-phase PV grid-connected inverters," Int. Journal of Computer and Electrical Engineering, vol. 5, no. 3, June 2013.
56. Reznik A., Simoes M. G., Durra A. Al., Muyeen S. M., "LCL Filter Design and Performance Analysis for Small Wind Turbine Systems," in Power Electronics and Machines in Wind Applications (PEMWA), IEEE, 2012, pp. 1-7.
57. Sahu I., Gadanayak D. A., "Comparison between two types of current control techniques applied to shunt active power filters and development of a novel fuzzy logic controller to improve SAPF performance," International Journal of Engineering Research and Development, vol. 2, no. 4, pp. 1-10, July 2012.
58. Shimada M., Miyaji Y., Kaneko T., Suzuki K., "Energy-saving technology for railway traction systems using onboard storage batteries," Hitachi Review, vol. 61, no. 7, pp. 312-318, 2012.
59. Shishime K, "Practical applications of the railway static power conditioner (RPC) for conventional railways," MEIDEN Review, no. 156, pp. 38-41, 2012.
60. Shu Z., Xie S., Li Q., "Single-phase back-to-back converter for active power balancing, reactive power compensation, and harmonic filtering in traction power system," IEEE Trans. on Power Electronics, vol. 26, no. 2, pp. 334-343, Feb. 2011.
61. Sikora A., Kulesz B., "Properties of novel traction polyphase rectifier transformer," in Proc. XXth International Conference on Electrical Machines, Sept. 2012, pp. 2139-2144.
62. Singh B., Solanki J., "An implementation of an adaptive control algorithm for a three-phase shunt active filter," IEEE Trans. Ind. Electron., vol. 56, no. 8, Aug. 2009.
63. Solis O.,Castro F.,Bukhin L., Pham K., Turner D., Thompson G., "Saving money every day: La metro subway wayside energy storage substation, in Proc. JRC, 2015 Joint Rail Conference, March 23 – 26, San Jose CA., 2015.
64. Sujatha C., Sekhar K. C., Boppa R. T., "Performance of fuzzy based shunt active power filter using indirect current control technique," International Journal of Science and Research, vol. 3 no. 12, pp. 810-816, Dec. 2014.
65. Suru V., Popescu M., Deaconu I., "Study of indirect current control methods for urban traction active dc substations," Annals of the University of Craiova Electrical Engineering series, no. 39, pp. 157-163, 2015.
66. Takahashi H., Kato T., Ito T., Gunji F., "Energy storage for traction power supply systems," Hitachi Review, vol. 57 no. 1, pp. 28-32, 2008.
67. Tang Y., Loh P.C., Wang P., Choo F.H., Gao F., Blaabjerg F., "Generalized design of high performance shunt active power filter with output LCL filter," IEEE Trans. Ind. Electron., vol. 59, no. 3, pp. 1443-1452, March 2012.
68. Thong M., Cheong A., "Energy efficiency in Singapore's rapid transit system," JOURNEYS I, pp. 38-47, May 2012.

69. Trinh Q.N., Lee H.H., "An advanced current control strategy for three-phase shunt active power filters," IEEE Trans. Ind. Electron., vol. 60, no. 12, pp. 5400-5410, Dec. 2013.
70. Wang X., Blaabjerg F., Loh P.C., "Grid-Current-Feedback Active Damping for LCL Resonance in Grid-Connected Voltage Source Converters," IEEE Trans. Power Electron., vol. 31, no. 1, pp. 213-223, Jan. 2016.
71. Warin Y., Lanselle R., Thiounn M., "Active substation," World Congress on Railway Research, Lille, France, May 2011.
72. Yang X.,Li X.,Ning B., Tang T., "A survey on energy-efficient train operation for urban rail transit," IEEE Transactions on Intelligent Transportation Systems, vol. 17, issue 1, pp. 2-13, Jan. 2016.
73. ***, "London underground energy recovery trial proves successful," http://www.railwaygazette.com/news/urban/single-view/view/london-underground-energy-recovery-trial-proves-successful.html.
74. ***, "RE-USE - Reducing the CO2 emission of urban guided systems through the full recovery of the brake Energy of metro trains." LIFE11 ENV/FR/000756, http://ec.europa.eu/environment/life/project/Projects/index.cfm?fuseaction=search.dspPage&n_proj_id=4438&docType=pdf
75. ***, Siemens, "Sitras TCI–Thyristor controlled inverter for DC traction power supply," Siemens AG 2010, <https://w3.usa.siemens.com/ mobility/us/Documents/en/rail-solutions/railway-electrification/dc-traction-power-supply/sitras-tci-en.pdf>
76. ***,Los Angeles county metropolitan transportation authority, "Sustainable Rail Plan," May 2013, http://media.metro.net/about_us/sustainability /images/sustainable_rail_plan_final_clean_submitted.pdf.

Alexandru Bitoleanu
Faculty of Electrical Engineering, University of Craiova, Str. A. I. Cuza nr.13, Craiova, Romania
alex.bitoleanu@em.ucv.ro